Surface Plasmon Resonance Waveguide Sensor in the Terahertz Regime

Jun Shibayama, *Member, IEEE, Member, OSA*, Keisuke Shimizu, Junji Yamauchi, *Fellow, IEEE, Member, OSA*, and Hisamatsu Nakano, *Life Fellow, IEEE*

***Abstract*—A surface plasmon resonance (SPR) waveguide sensor with a thin InSb layer adopted for the sensing section is proposed in the terahertz region. First, the eigenmode analysis is carried out for the sensing section with water as an analyte. The surface plasmon polariton eigenmodes are shown to exist in the sensing section, and the SPR is expected to be maximum around 1.28 THz at 300 K. Next, the performance of the sensor is investigated using the finite-difference time-domain method, with special attention to the treatment of the interface between InSb and water. As expected, the SPR absorption is found to become maximum at 1.26 THz. Furthermore, the SPR response is examined, in which an ability is shown to detect a temperature variation ranging from 280 to 320 K. As an application, final consideration is given to the possibility of detecting a mixture of an organic solvent and water.**

***Index Terms*—Frequency-dependent finite-difference time-domain (FDTD) method, indium antimonide (InSb), surface plasmon polariton (SPP), surface plasmon resonance sensor, terahertz waves, trapezoidal recursive convolution.**

I. Introduction

AT OPTICAL frequencies, surface plasmon resonance (SPR) sensors have extensively been studied and already been available commercially [1]–[4]. The SPR sensors utilize surface plasmon polariton (SPP) waves excited along the metal/dielectric interface, the characteristics of which are quite sensitive to the properties of an analyte.

For conventional SPR sensors, the Kretschmann configuration [5] has widely been used due to its simple structure consisting of a prism coated with a thin metal layer. Unfortunately, the Kretschmann configuration is not suitable for monolithic integration into optical circuits, because of the bulk structure of the prism. Recently, SPR waveguide-based sensors have also been studied [6]–[10], since monolithic integration can be achieved using the fabrication techniques for optical devices. We have theoretically investigated several SPR waveguide sensors and improved their performance [11]–[14].

The SPR sensors at optical frequencies can detect, for example, protein-DNA interactions [15] and antigen-antibody complex reactions [16]. At THz frequencies, on the other hand, vibrational modes of hydrogen exist around 1 THz. Moreover, THz waves are highly absorbed by pure water while not by an aqueous solution. Therefore, the use of THz waves has also attracted attention in the field of biochemistry.

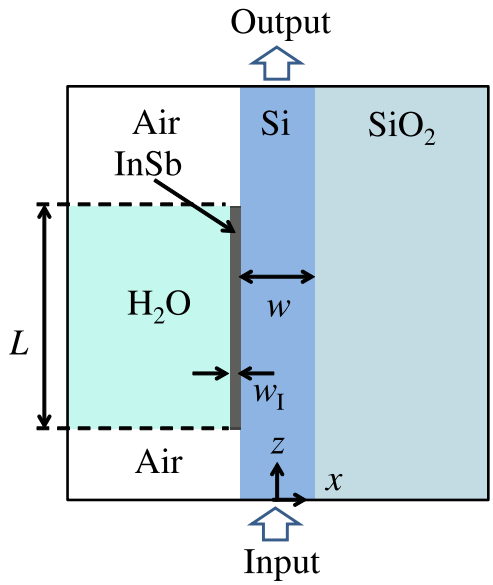

Fig. 1. Configuration of an SPR waveguide sensor.

At THz frequencies, the SPP waves cannot be supported along the metal/dielectric interface. This is because THz frequencies are far below the plasma frequency of metal, resulting in negligible penetration of the electromagnetic fields. Here, we should note that a semiconductor material such as indium antimonide (InSb) exhibits plasma frequencies in the THz band [17]–[20]. Fortunately, this allows the propagation of THz SPP waves along the InSb/dielectric interface. With these SPP waves, several groups have studied temperature-dependent THz functional devices [21]–[27]. However, little attention has been paid to investigating an SPR waveguide sensor in the THz regime.

In this paper, we propose a THz SPR waveguide sensor using a thin InSb layer adopted for the sensing section (see Fig. 1). In [28], we have briefly mentioned the SPR waveguide sensor with water as an analyte. We here present how the finite-difference time-domain (FDTD) method is applied to the analysis of the sensor structure, and discuss the characteristics of the sensor in great detail.

After reviewing the frequency- and temperature-dependent permittivities of InSb and water, we perform the eigenmode analysis for the sensing section. Numerical results show that SPP eigenmodes exist in the sensing section with water. The overlap

Manuscript received September 19, 2015; revised February 13, 2016; accepted March 7, 2016. Date of publication March 8, 2016; date of current version April 11, 2016. This work was supported in part by MEXT, Grant-in-Aid for Scientific Research (C) (15K06035).

The authors are with the Faculty of Science and Engineering, Hosei University, Tokyo 184-8584, Japan (e-mail: shiba@hosei.ac.jp; keisuke.shimizu.7a@stu.hosei.ac.jp; j.yma@hosei.ac.jp; hymat@hosei.ac.jp).

Color versions of one or more of the figures in this paper are available online at http://ieeexplore.ieee.org.

Digital Object Identifier 10.1109/JLT.2016.2539974

integral calculations between the SPP and input eigenmodes indicate that the SPR absorption peak is expected around 1.28 THz at 300 K.

Then, we analyze the sensor using the frequency-dependent FDTD method, paying attention to the treatment of the interface between InSb and water. To maintain higher numerical accuracy for a small field amplitude, the interface is expressed by the Drude model possessing an average permittivity of InSb and water. As expected from the eigenmode analysis, the maximum SPR absorption is found to occur at 1.26 THz. Furthermore, the SPR response is examined for a temperature variation ranging from 280 to 320 K.

Final consideration is given to the application of the present SPR sensor to detecting an aqueous solution of an organic solvent. In particular, we consider an acetonitrile-water solution, showing an ability to detect their volume fractions.

II. Permittivities of InSb and Water

The permittivities of InSb and water exhibit frequency and temperature dependence. We review the dispersion models for these two materials.

The permittivity of InSb is often expressed by the Drude model as [19]–[27]

$$\varepsilon_{\mathrm{I}}(\omega) = \varepsilon_{\mathrm{I}\infty} + \frac{\omega_p^2}{\omega\,(j\Gamma - \omega)} \tag{1}$$

where $\varepsilon_{\mathrm{I}\infty}(=15.7)$ is the high-frequency permittivity, ω is the angular frequency, ω_p is the plasma frequency, and Γ is the electron collision rate. The latter two are defined as

$$\omega_p = \sqrt{\frac{N_d e^2}{\varepsilon_0 m^*}} \tag{2}$$

$$\Gamma = \frac{e}{m^* \mu} \tag{3}$$

where N_d is the free carrier concentration, e is the elementary charge, ε_0 is the vacuum permittivity, m^* is the effective mass of charge carrier, and μ is the mobility of charge carrier. The electron effective mass of InSb is $0.014m_0$, where m_0 is the electron mass. For InSb, N_d and μ can be obtained as [26]

$$N_d = 6 \times 10^{14} T^{3/2} e^{-0.29/2kT}\ (\mathrm{cm}^{-3}) \tag{4}$$

$$\mu = 7.7 \times 10^4 \left(\frac{T}{300}\right)^{-1.66}\ (\mathrm{cm}^2/\mathrm{Vs}) \tag{5}$$

where T and k are the temperature and Boltzmann constant, respectively.

Fig. 2 shows ω_p and Γ as a function of temperature obtained from (2) and (3) [26], in which the symbols denote the data available from [19]. A close correspondence can be seen to exist between the results from [26] and those from [19]. Since we investigate the characteristics of the sensor for an arbitrary temperature, the expressions (2) and (3) are used throughout this paper.

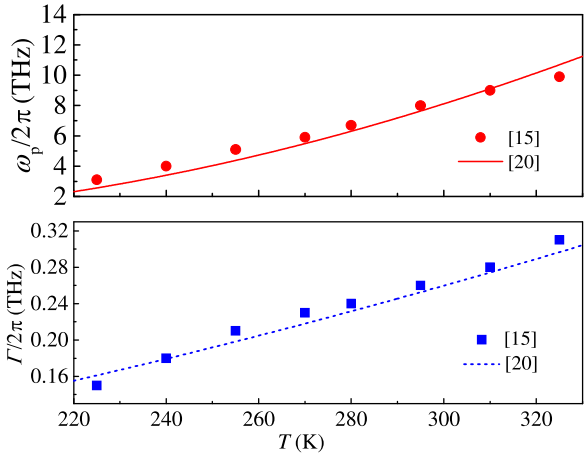

Fig. 2. ω_p and Γ adopted for the Drude model of InSb.

The relative permittivity of water is expressed by the following double Debye model [29]:

$$\varepsilon_w(\omega) = \varepsilon_2 + \frac{\varepsilon_0 - \varepsilon_1}{1 + \frac{j\omega}{2\pi\gamma_1}} + \frac{\varepsilon_1 - \varepsilon_2}{1 + \frac{j\omega}{2\pi\gamma_2}} \tag{6}$$

where

$$\begin{aligned}
\varepsilon_0 &= 77.66 - 103.3\theta \\
\varepsilon_1 &= 0.0671\varepsilon_0 \\
\varepsilon_2 &= 3.52 + 7.52\theta \\
\gamma_1 &= 20.20 + 146.4\theta + 316\theta^2 \\
\gamma_2 &= 39.8\gamma_1 \\
\theta &= 1 - \frac{300}{T}
\end{aligned}$$

in which ε_0 is the static dielectric constant of water, ε_1 and ε_2 are respectively the first and second high-frequency constants, γ_1 and γ_2 are respectively the primary and secondary relaxation frequencies, and θ is the modified relative inverse variable. The permittivity from (6) follows the experimental data quite well [29]. The above parameters of InSb and water are incorporated into the frequency-dependent FDTD method to be used in IV.

III. Eigenmode Analysis of the Sensing Section

The sensing performance mainly depends on the propagation characteristics of the SPP waves. It is therefore important to know the SPP characteristics in the sensing section at the THz frequencies. Here, we carry out the eigenmode analysis in the sensing section using the imaginary-distance finite-difference beam-propagation method (BPM) [30], [31]. The imaginary-distance procedure efficiently provides eigemodes, in which the coordinate in the propagation direction of the BPM is changed to $j\tau$.

The sensor configuration is shown in Fig. 1, in which the thin InSb layer is placed on the Si/SiO_2 waveguide and water is chosen as an analyte. In this paper, Si and SiO_2 are assumed to be temperature-independent and lossless materi-

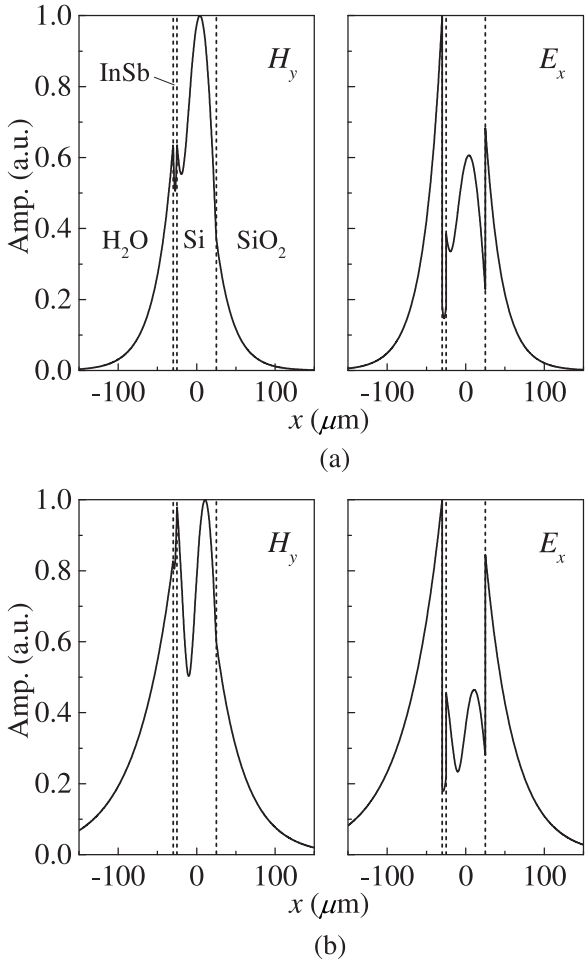

Fig. 3. SPP eigenmode fields at 1.28 THz. (a) First mode. (b) Second mode.

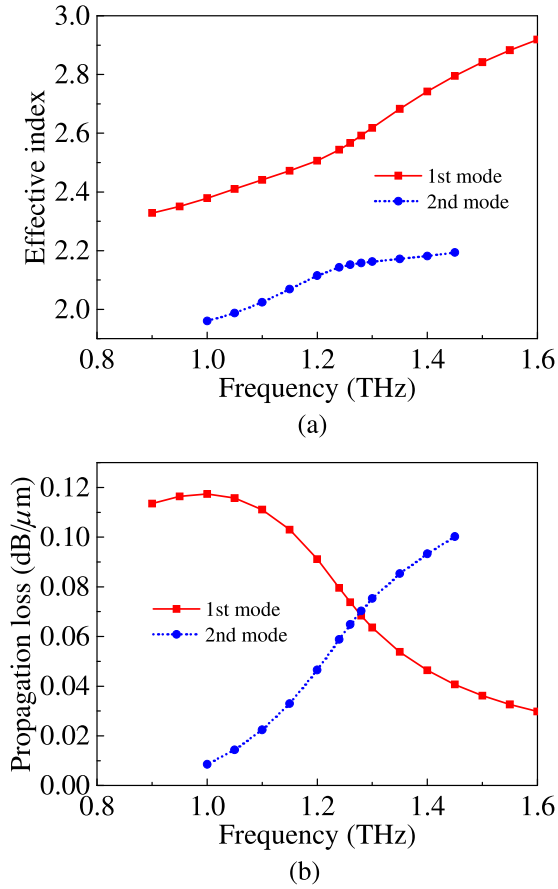

Fig. 4. Results of the eigenmode analysis. (a) Effective index. (b) Propagation loss.

als, and their relative permittivities are chosen to be 3.4^2 [32] and 1.95^2 [33], respectively. The configuration parameters are $w = 50$ μm, $w_{\mathrm{I}} = 5$ μm and $L = 400$ μm (preliminary calculations show that a thickness of $w_{\mathrm{I}} = 5$ μm exhibits a strong SPR resonance over a wide frequency range). The temperature is set at $T = 300$ K.

As a result of the analysis, we have observed three SPP modes in the sensing section. Of them, the lowest mode exhibits a large propagation loss and a negligible coupling from the input eigenmode. Therefore, we only discuss the two higher eigenmodes, in which one with a larger effective index is called the first mode and the other the second mode.

The two SPP eigenmode fields (H_y and E_x components) at 1.28 THz are illustrated in Fig. 3, the field amplitude of which is normalized to its maximum value. It is seen that the field amplitude is appreciably enhanced around the thin InSb layer. This results in a large evanescent field in the analyte, leading to an ability to detect the analyte property. The effective index and propagation loss versus frequency are shown in Fig. 4. As can be seen, the effective indexes for both modes increase with frequency, while the propagation losses are almost the same at $\simeq$1.28 THz.

To estimate how much the input eigenmode is coupled to each of the two SPP modes, we calculate the overlap integral between them. The overlap integral is defined as

$$O.I. = \frac{|\int \phi_{\mathrm{SPP}} \cdot \phi^*_{\mathrm{Input}} dx|^2}{\int |\phi_{\mathrm{SPP}}|^2 dx \int |\phi_{\mathrm{Input}}|^2 dx} \tag{7}$$

where ϕ_{SPP} is the SPP mode field in the sensing section and ϕ_{Input} is the input eigenmode field. Although either electric or magnetic mode field can be used for this calculation, the magnetic field is used in this paper.

Fig. 5 depicts the overlap integral, in which the total value of the two results is also included. It is seen that the total value reaches 0.9 at frequencies of higher than 1.2 THz and it becomes 0.98 at 1.28 THz where the propagation losses of the two modes are almost the same. Note for the SPR sensor in the optical regime that the SPR absorption becomes maximum around the frequency at which the propagation losses are almost the same for the two SPP modes [12]. For the present sensor, an SPR absorption peak is also expected to exist around 1.28 THz, where most of the input eigenmode is coupled to the two SPP modes, and the two propagation losses are almost the same.

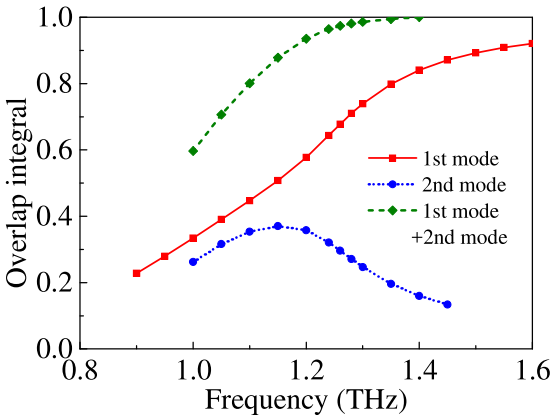

Fig. 5. Overlap integral.

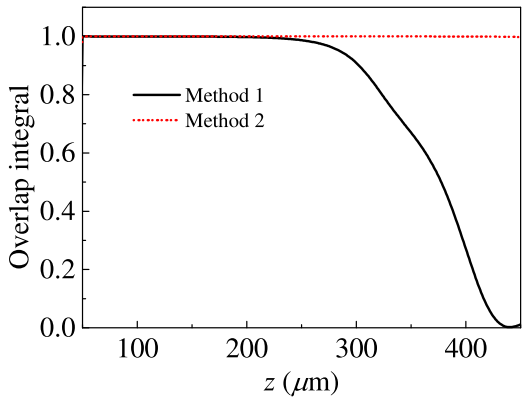

Fig. 6. Overlap integral.

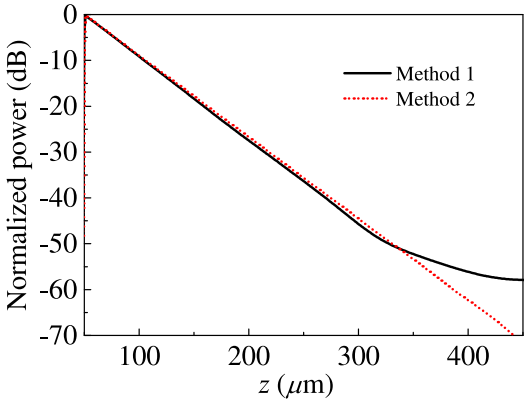

Fig. 7. Normalized power.

IV. FDTD Analysis of the SPR Waveguide Sensor

Since the SPP characteristics have been made clear from the eigenmode analysis, we next analyze the SPR waveguide sensor using the FDTD method. For the FDTD analysis of dispersive media, the frequency-dependent version is required. In this paper, we employ the frequency-dependent FDTD method based on the simple trapezoidal recursive convolution technique [34]–[36].

A. Treatment of the Interface Between InSb and Water

Note for the present sensor that the Drude and Debye models form a boundary in the sensing section. Although the boundary between two different dispersive materials should be carefully implemented for the frequency-dependent FDTD analysis, little discussion has been made on its treatment so far. In what follows, we discuss how to treat the interface between InSb and water.

For plasmonic devices, a dispersive material (e.g., metal at optical frequencies) is usually surrounded by a nondispersive one (normal dielectric). In this case, we have two techniques for treating its boundary. One is to calculate the electric field on the boundary having the dispersion model and that having nondispersion model, followed by averaging those electric fields [37]. The other is to use a dispersion model possessing an averaged permittivity of the dispersion and nondispersion models [38], [35]. Note that these two techniques have not yet been fully examined for the case where two different dispersion models form a boundary. Therefore, we here investigate the performance of these two techniques for the boundary between InSb and water. For convenience, the former and latter techniques are called Method 1 and Method 2, respectively.

Following Method 1, we average the electric field obtained from the Drude model (1) for InSb and that from the Debye model (6) for water on their boundary. For Method 2, we assume that the permittivity on the boundary is expressed by the Drude model with an averaged permittivity. We calculate the complex permittivities of InSb and water from (1) and (6) at a specific frequency to be investigated, and then average these permittivities. With the solution of simultaneous equations from the assumed Drude model and the averaged permittivities, we obtain the plasma frequency and the electron collision rate of the assumed Drude model with the averaged permittivity.

To examine the performance of the two methods, we calculate the overlap integral between the eigenmode and the propagating field in the sensing section at 300 K. If the field is accurately calculated, the eigenmode field does not deform with the overlap integral remaining constant (unity). Fig. 6 shows the overlap integral versus propagation distance, in which the lowest eigenmode of the sensing section at 1 THz is utilized as an input field. It is seen that the overlap integral of Method 1 deviates from unity around 200 μm. Since the boundary condition depends on the field amplitude, the numerical accuracy of Method 1 cannot be maintained for a small field amplitude. For Method 2, on the other hand, the overlap integral keeps unity up to 450 μm. This is because the averaged permittivity does not depend on the field amplitude, leading to accurate results for a longer propagation distance.

We next calculate the normalized power remaining in the computation region to know to what extent the numerical accuracy is maintained with small power. Fig. 7 depicts the normalized power versus propagation distance. From Figs. 6 and 7, Method 1 and 2 maintain their accuracy with a normalized power of $\simeq -25$ and -70 dB, respectively.

Although Method 1 cannot maintain its accuracy with a small field amplitude, the implementation is relatively easy and its application to the calculations of frequency responses

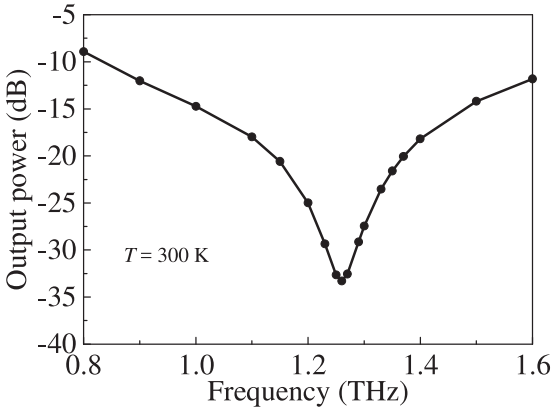

Fig. 8. Output power at $T = 300$ K.

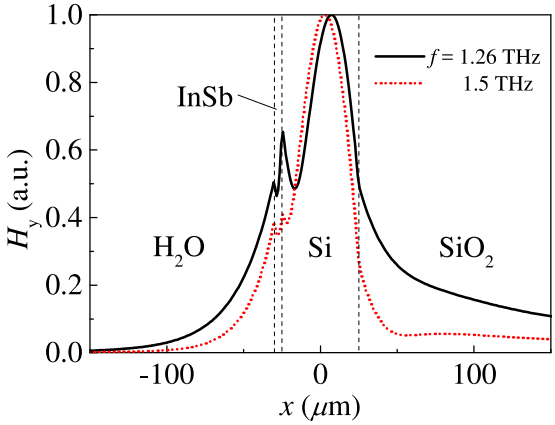

Fig. 10. Propagating fields at $z = 200$ μm.

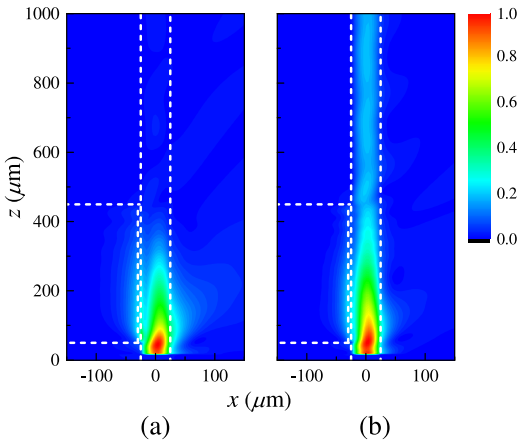

Fig. 9. Field distributions at $T = 300$ K. H_y components are displayed.

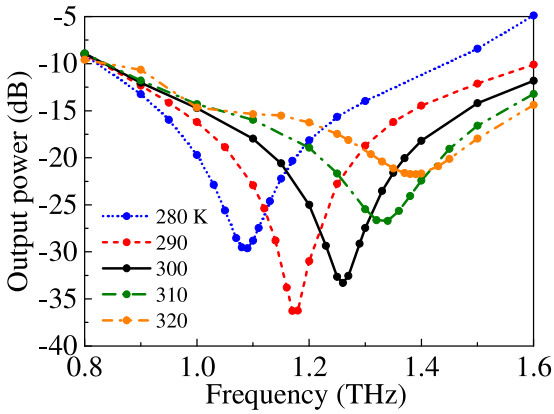

Fig. 11. SPR response for various temperatures.

is also straightforward. While Method 2 provides higher numerical accuracy even with a small field amplitude, the derivation of parameters needs to solve simultaneous equations. In this paper, we resort to Method 2 to handle a small field amplitude particularly at the SPR frequency.

B. SPR Response

We investigate the SPR response of the sensor, in which the eigenmode of the input waveguide is launched and the output power (guided mode power) is evaluated. Fig. 8 shows the SPR response at $T = 300$ K. As expected from the eigenmode analysis, the maximum SPR absorption is found to occur at 1.26 THz. This frequency is close to that where the propagation losses of the two SPP mode are the same as each other, as shown in Fig. 4(b). Consequently, the eigenmode analysis is useful for predicting the SPR frequency of a waveguide sensor.

Fig. 9 illustrates the field distributions for the resonant peak at 1.26 THz and the off-resonant peak at 1.5 THz. It is observed that the input THz wave rapidly loses its power at 1.26 THz due to the strong SPR, when compared with the case at 1.5 THz. Here, we check the amplitude of the SPP in the sensing section. Fig. 10 shows the propagating fields (H_y components) at $z = 200$ μm, in which the field is normalized to its maximum value in the core. It is seen that the SPP amplitude at 1.26 THz excited around the InSb layer is higher than that at 1.5 THz, resulting in a large propagation loss.

Since we have confirmed that the sensor shows an SPR response, we next investigate the temperature dependence of the sensor. The SPR response is shown in Fig. 11, in which the temperature ranges from 280 to 320 K. As can be seen, the peak frequency becomes higher as the temperature is increased. Note that the real part of the InSb relative permittivity significantly varies from -16.3 to -35.3 with the temperature increase. As a result, the shift of the peak frequency is mainly attributed to a variation of the resonance condition, resulting from the InSb permittivity change.

Fig. 12 depicts the peak frequency as a function of temperature. It is shown that the peak frequency varies almost linearly with temperature. From this result, the sensitivity is estimated to be about 7.5×10^{-3} THz/K, which is higher than that reported in [27] (1.425×10^{-3} THz/K). This difference is probably because water with the temperature-dependent permittivity (6) enhances the sensitivity of the present sensor. As a result, the temperature determines the SPR peak frequency, showing a possibility to act as a temperature sensor.

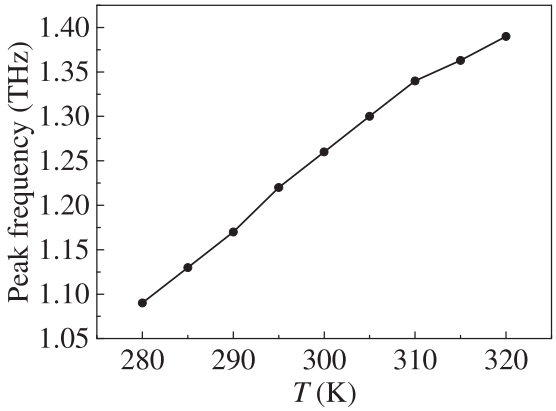

Fig. 12. Peak frequency versus temperature.

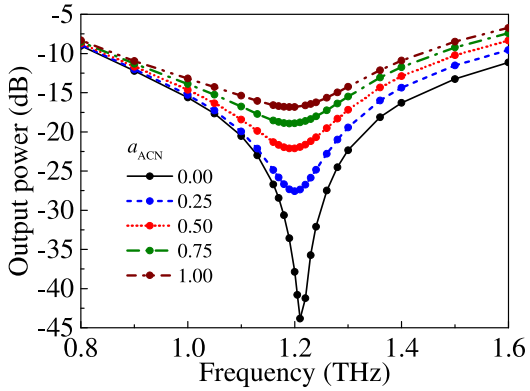

Fig. 13. SPR response for various volume fractions.

Note that a structure for containing water has not been considered in this paper. One candidate for it is to use an analyte container that is a concave section made in the upper cladding [39]. We will apply this structure to a practical three-dimensional sensor in our future work.

V. Detection of Mixture of Organic Solvent and Water

Final consideration is given to the application of detecting a mixture of an organic solvent and water using the present SPR waveguide sensor. We here consider an acetonitrile-water solution, which has received continuous attention for decades due to a wide variety of applications [40]–[43].

The permittivity for mixtures of acetonitrile-water is expressed by the double Debye model, the parameters of which are found in [41]. Fig. 13 shows the SPR response at $T = 293$ K for several volume fractions denoted by a_{ACN}. It is found that as a_{ACN} is increased the output power also increases (the real part of the relative permittivity of water is reduced from 4.00 for $a_{\mathrm{ACN}} = 0$ to 2.5 for $a_{\mathrm{ACN}} = 1.0$, while the imaginary part is almost constant). This variation of the output power is related to the strength of the SPR. That is, the SPR is strong for $a_{\mathrm{ACN}} = 0$, resulting in the reduced output power. For $a_{\mathrm{ACN}} = 1.0$, the SPR becomes weak, decreasing the absorption of THz waves with a concomitant increase of the output power (although not illustrated, the amplitude of the SPP around the InSb becomes low for the reduced relative permittivity of water). Unlike the results of Figs. 11 and 12, the peak frequency change is quite small. This is due to the fixed temperature at $T = 293$ K.

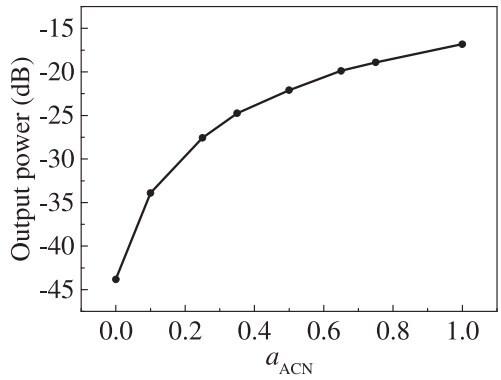

Fig. 14. Output power versus volume fraction.

As mentioned, aqueous solutions decrease the absorption of THz waves. Therefore, we focus on how the output power increases with an increase in the volume fractions of acetonitrile. The minimum output power versus a_{ACN} is depicted in Fig. 14. It is seen that the minimum power increases from -43.7 to -16.7 dB with a_{ACN} being increased from 0 to 1. It is interesting to note that the sensitivity is higher when a_{ACN} is small. Measuring the minimum output power is expected to detect the volume fractions of acetonitrile and water.

VI. Conclusion

This paper has presented a THz SPR waveguide sensor with a thin InSb layer being adopted for the sensing section. First, the InSb and water permittivities expressed, respectively, by the Drude and Debye models are reviewed, which are incorporated into the frequency-dependent FDTD method. Next, the SPP eigenmodes are shown to exist in the sensing section. From the overlap integral calculations between the SPP and input eigenmodes, the SPR is expected to be maximum around 1.28 THz. Then, the sensor is analyzed using the FDTD method with special attention to the treatment of the InSb/water interface. The FDTD analysis shows that the SPR absorption becomes maximum at 1.26 THz, which is close to that expected from the eigenmode analysis. The SPR response is further investigated for a temperature variation, showing an ability to detect the temperature of water ranging from 280 to 320 K. Finally, a mixture of an organic solvent and water is examined, the volume fraction of which is detectable with measuring the local minimum power at the SPR frequency. Consequently, an SPR waveguide sensor can be realized with a thin InSb layer even at THz frequencies. Analysis of a practical three-dimensional sensor with a analyte container will be the subject of future work.

ACKNOWLEDGMENT

The authors would like to thank the reviewers for their valuable comments and suggestions.

REFERENCES

[1] J. Homola, S. S. Yee, and G. Gauglitz, "Surface plasmon resonance sensors: Review," *Sens. Actuators B*, vol. 54, pp. 3–15, Jan. 1999.
[2] J. Homola, "Present and future of surface plasmon resonance biosensors," *Anal. Bioanalytical Chem.*, vol. 377, no. 3, pp. 528–539, Oct. 2003.
[3] L. M. Zhang and D. Uttamchandani, "Optical chemical sensing employing surface-plasmon resonance," *Electron. Lett.*, vol. 24, no. 23, pp. 1469–1470, Nov. 1988.
[4] K. Matsubara, S. Kawata, and S. Minami, "Optical chemical sensor based on surface-plasmon measurement," *Appl. Opt.*, vol. 27, no. 6, pp. 1160–1163, Mar. 1988.
[5] E. Kretschmann, "Die Bestimmung optischer Konstanten von Metallen durch Anregung von Oberflächenplasmaschwingungen" *Z. Physik*, vol. 241, no. 4, pp. 313–324, 1971.
[6] J. Čtyroký, J. Homola, P. V. Lambeck, S. Musa, H. J. W. M. Hoekstra, R. D. Harris, J. S. Wilkinson, B. Usievich, and N. M. Lyndin, "Theory and modelling of optical waveguide sensors utilising surface plasmon resonance," *Sens. Actuators B*, vol. 54, nos. 1/2, pp. 66–73, Jan. 1999.
[7] J. Čtyroký, J. Homola, and M. Skalsky, "Tuning of spectral operation range of a waveguide surface plasmon resonance sensor," *Electron. Lett.*, vol. 33, no. 14, pp. 1246–1248, Jul. 1997.
[8] C. R. Lavers and J. S. Wilkinson, "A wave-guide-coupled surface-plasmon sensor for an aqueous environment," *Sens. Actuators B*, vol. 22, no. 1, pp. 75–81, Oct. 1994.
[9] R. D. Harris and J. S. Wilkinson, "Waveguide surface plasmon resonance sensors," *Sens. Actuators B*, vol. 29, nos. 1–3, pp. 261–267, Oct. 1995.
[10] M. N. Weiss, R. Srivastava, H. Groger, P. Lo, and S. F. Luo, "A theoretical investigation of environmental monitoring using surface plasmon resonance waveguide sensors," *Sens. Actuators A*, vol. 51, pp. 211–217, Nov. 1996.
[11] J. Shibayama, T. Takeuchi, N. Goto, J. Yamauchi, and H. Nakano, "Numerical investigation of a Kretschmann-type surface plasmon resonance waveguide sensor," *J. Lightw. Technol.*, vol. 25, no. 9, pp. 2605–2611, Sep. 2007.
[12] J. Shibayama, S. Takagi, T. Yamazaki, J. Yamauchi, and H. Nakano, "Numerical analysis of waveguide-based surface plasmon resonance sensor with adsorbed layer using two- and three-dimensional beam-propagation methods," *IEICE Trans. Electron.*, vol. E90-C, no. 1, pp. 95–101, Jan. 2007.
[13] J. Shibayama, "A Kretschmann-type absorption-based surface plasmon resonance waveguide sensor," *Microw. Opt. Technol. Lett.*, vol. 50, no. 10, pp. 2497–2500, Oct. 2008.
[14] J. Shibayama, "Three-dimensional numerical investigation of an improved surface plasmon resonance waveguide sensor," *IEEE Photon. Technol. Lett.*, vol. 22, no. 9, pp. 643–645, May 2010.
[15] J. M. Brockman, B. P. Nelson, and R. M. Corn, "Surface plasmon resonance imaging measurements of ultrathin organic films," *Annu. Rev. Phys. Chem.*, vol. 51, pp. 41–63, Oct. 2000.
[16] L. G. Fägerstam, Å. Frostell, R. Karlsson, M. Kullman, A. Larsson, M. Malmqvist, and H. Butt, "Detection of antigen-antibody interactions by surface plasmon resonance. Application to epitope mapping," *J. Mol. Recognit.*, vol. 3, nos. 5/6, pp. 208–214, Oct.–Dec. 1990.
[17] J. Gómez Rivas, C. Schotsch, P. Haring Bolivar, and H. Kurz, "Enhanced transmission of THz radiation through subwavelength holes," *Phys. Rev. B*, vol. 68, pp. 201306-1–201306-4, Nov. 2003.
[18] J. Gómez Rivas, M. Kuttge, H. Kurz, P. Haring Bolivar, and J. A. Sánchez-Gil, "Low-frequency active surface plasmon optics on semiconductors," *Appl. Phys. Lett.*, vol. 88, no. 8, pp. 082106-1–082106-3, Feb. 2006.
[19] J. A. Sánchez-Gil and J. Gómez Rivas, "Thermal switching of the scattering coefficients of terahertz surface plasmon polaritons impinging on a finite array of subwavelength grooves on semiconductor surfaces," *Phys. Rev. B*, vol. 73, no. 20, pp. 205410-1–205410-8, May 2006.
[20] T. H. Isaac, W. L. Barnes, and E. Hendry, "Determining the terahertz optical properties of subwavelength films using semiconductor surface plasmons," *Appl. Phys. Lett.*, vol. 93, no. 24, pp. 241115-1–241115-3, Dec. 2008.
[21] M. K. Chen, Y. C. Chang, C. E. Yang, Y. Guo, J. Mazurowski, S. Yin, P. Ruffin, C. Brantley, E. Edwards, and C. Luo, "Tunable terahertz plasmonic lenses based on semiconductor microslits," *Microw. Opt. Tech. Lett.*, vol. 52, no. 4, pp. 979–981, Apr. 2010.
[22] B. Hu, Q. J. Wang, S. W. Kok, and Y. Zhang, "Active focal length control of terahertz slitted plane lenses by magnetoplasmons," *Plasmonics*, vol. 7, no. 2, pp. 191–199, Jun. 2012.
[23] B. Hu, Q. J. Wang, and Y. Zhang, "Broadly tunable one-way terahertz plasmonic waveguide based on nonreciprocal surface magneto plasmons," *Opt. Lett.*, vol. 37, no. 11, pp. 1895–1897, Jun. 2012.
[24] J. Tao, B. Hu, X. Y. He, and Q. J. Wang, "Tunable subwavelength terahertz plasmonic stub waveguide filters," *IEEE Trans. Nanotech.*, vol. 12, no. 6, pp. 1191–1197, Nov. 2013.
[25] J. Shibayama, Y. Wada, J. Yamauchi, and H. Nakano, "Application of the explicit and implicit FDTD methods to the analysis of a terahertz plasmonic grating," in *Proc. Prog. Electromag. Res. Symp. Abstracts*, Guangzhou, China, Aug. 2014, pp. 1904–1922.
[26] Q Wang, Q. Tang, D. Zhang, Z. Wang, and Y. Huang, "Tunable terahertz spectral filter based on temperature controlled subwavelength InSb grating," *Superlattices Microstruct.*, vol. 75, pp. 955–961, Nov. 2014.
[27] H. Liu, G. Ren, Y. Gao, Y. Lian, Y. Qi, and S. Jian, "Tunable subwavelength terahertz plasmon-induced transparency in the InSb slot waveguide side-coupled with two stub resonators," *Appl. Opt.*, vol. 54, no. 13, pp. 3918–3924, May 2015.
[28] J. Shibayama, J. Yamauchi, and H. Nakano, "FDTD analysis of several terahertz devices using surface plasmon polariton waves," in *Proc. IEEE 4th Asia-Pacific Conf. Antennas Propag.*, Bali Island, Indonesia, Jul. 2015, pp. 222–223.
[29] H. J. Liebe, G. A. Hufford, and T. Manabe, "A model for the complex permittivity of water at frequencies below 1 THz," *Int. J. Infrared Millimeter Waves*, vol. 12, no. 7, pp. 659–675, Jul. 1991.
[30] D. Yevick and B. Hermansson, "New formulations of the matrix beam propagation method: Application to rib waveguides," *IEEE J. Quantum Electron.*, vol. 25, no. 2, pp. 221–229, Feb. 1989.
[31] J. Shibayama, T. Yamazaki, J. Yamauchi, and H. Nakano, "Eigenmode analysis of a light-guiding metal line loaded on a dielectric substrate using the imaginary-distance beam-propagation method," *J. Lightw. Technol.*, vol. 23, no. 3, pp. 1533–1539, Mar. 2005.
[32] D. Grischkowsky, S. Keiding, M. van Exter, and C. Fattinger, "Far-infrared time-domain spectroscopy with terahertz beams of dielectrics and semiconductors," *J. Opt. Soc. Amer. B*, vol. 7, no. 10, pp. 2006–2015, Oct. 1990.
[33] Y. H. Avetisyan, H. S. Hakobyan, and V. R. Tadevosyan, "Analysis of plasmon terahertz waveguide formed by a dielectric ridge on semiconductor surface," *J. Contemp. Phy.*, vol. 46, no. 5, pp. 361–367, Oct. 2011.
[34] R. Siushansian and J. LoVetri, "A comparison of numerical techniques for modeling electromagnetic dispersive media," *IEEE Microw. Guided Wave Lett.*, vol. 5, no. 12, pp. 426–428, Dec. 1995.
[35] J. Shibayama, R. Ando, A. Nomura, J. Yamauchi, and H. Nakano, "Simple trapezoidal recursive convolution technique for the frequency-dependent FDTD analysis of a Drude-Lorentz model," *IEEE Photon. Technol. Lett.*, vol. 21, no. 2, pp. 100–102, Jan. 2009.
[36] J. Shibayama, A. Nomura, R. Ando, J. Yamauchi, and H. Nakano, "A frequency-dependent LOD-FDTD method and its application to the analyses of plasmonic waveguide devices," *IEEE J. Quantum Electron.*, vol. 46, no. 1, pp. 40–49, Jan. 2010.
[37] T. Arima and T. Uno, "Boundary treatment method of dispersive materials analysis by FDTD method" *Trans. IEICE*, vol. J91-B, no. 9, pp. 1066–1068, Sep. 2008.
[38] Y. Zhao, P. Belov, and Y. Hao, "Accurate modeling of the optical properties of left-handed media using a finite-difference time-domain method," *Phys. Rev. E*, vol. 75, no. 3, pp. 037602-1–037602-4, Mar. 2007.
[39] T. Yoshimura, J. Yamauchi, J. Shibayama, and H. Nakano, "Three-dimensional BPM analysis of a Kretschmann-type SPR sensor with an analyte container," in *Proc. IEICE Soc. Conf.*, Sep. 2012, C-3-24, p. 141.
[40] J. J. Ramsden, S. E. Webber, and M. Graetzel, "Luminescence of colloidal cadmium sulfide particles in acetonitrile and acetonitrile/water mixtures," *J. Phys. Chem.*, vol. 89, no. 13, pp. 2740–2743, Jun. 1985.
[41] D. S. Venables and C. A. Schmuttenmaer, "Far-infrared spectra and associated dynamics in acetonitrile-water mixtures measured with femtosecond THz pulse spectroscopy," *J. Chem. Phys.*, vol. 108, no. 12, pp. 4935–4944, Mar. 1998.
[42] T. Takamuku, M. Tabata, A. Yamaguchi, J. Nishimoto, M. Kumamoto, H. Wakita, and T. Yamaguchi, "Liquid structure of acetonitrile-water mixtures by x-ray diffraction and infrared spectroscopy," *J. Phys. Chem. B*, vol. 102, no. 44, pp. 8880–8888, Oct. 1998.

[43] N. Y. Tan, R. Li, P. Bräuer, C. D'Agostino, L. F. Gladden, and J. A. Zeitler, "Probing hydrogen-bonding in binary liquid mixtures with terahertz time-domain spectroscopy: A comparison of Debye and absorption analysis," *Phys. Chem.*, vol. 17, pp. 5999–6008, Jan. 2015.

Jun Shibayama (M'03) was born in Kashiwa, Japan, on July 1, 1969. He received the B.E., M.E., and Dr.Eng. degrees from Hosei University, Tokyo, Japan, in 1993, 1995, and 2001, respectively.

In 1995, he joined Opto-Technology Laboratory, Furukawa Electric Co., Ltd., Ichihara, Japan. He became an Assistant of Hosei University in 1999, where he is currently a Professor. His research interests include the numerical analysis of electromagnetic problems.

Dr. Shibayama is a Member of the OSA, ACES, and IEICE.

Keisuke Shimizu was born in Yokohama, Japan, on January 3, 1993. He received the B.E. degree from Hosei University, Tokyo, Japan, in 2015, where he is currently working toward the M.E. degree.

Mr. Shimizu is a Student Member of the Institute of Electronics, Information, and Communication Engineers of Japan.

Junji Yamauchi (M'84–SM'08–F'12) was born in Nagoya, Japan, on August 23, 1953. He received the B.E., M.E., and Dr. Eng. degrees from Hosei University, Tokyo, Japan, in 1976, 1978, and 1982, respectively.

From 1984 to 1988, he served as a Lecturer in the Department of Electrical Engineering, Tokyo Metropolitan Technical College. Since 1988, he has been a Member of the Faculty of Hosei University, where he is currently a Professor. His research interests include optical waveguides and circularly polarized antennas. He is the author of Propagating Beam Analysis of Optical Waveguides (London, U.K.: Research Studies Press, 2003).

Dr.Yamauchi is a Member of the Optical Society of America and the Institute of Electronics, Information, and Communication Engineers of Japan.

Hisamatsu Nakano (M'75–SM'87–F'92–LF'11) was born in Ibaraki, Japan, on April 13, 1945. He received the B.E., M.E., and Dr. Eng. degrees, all in electrical engineering, from Hosei University, Tokyo, Japan, in 1968, 1970, and 1974, respectively.

Since 1973, he has been a Member of the Faculty of Hosei University, where he is currently a Professor. His research interests include numerical methods for low- and high-frequency antennas and optical waveguides. He has published more than 200 refereed journal papers, more than 200 international symposium papers, and more than 750 national symposium papers. He is the author of a book entitled Helical and Spiral Antennas (New York, NY, USA: Wiley, 1987) and the coauthor of Analysis Methods of Electromagnetic Wave Problems, (vol. 2. Norwood, MA, USA: Artech House, 1986). In addition, he is the author of Helical and Spiral Antennas, Encyclopedia of Communications (New York, NY, USA: Wiley, 2002).

Dr. Nakano received the IEE International Conference on Antennas and Propagation Best Paper Award and the IEEE Transactions on Antennas and Propagation Best Application Paper Award (H. A. Wheeler Award) in 1989 and 1994, respectively. In 1992, he was elected as an IEEE Fellow for contributions to the design of spiral and helical antennas. In 2001, he received the Award of Distinguished Technical Communication (from the Society for Technical Communication, USA) and the Science and Technology Progress Award (from Hangzhou, China). He also received the Chen-To Tai Distinguished Educator Award (from the IEEE Antennas and Propagation Society) in 2006. He is an Associate Editor of several journals and magazines, such as *Electromagnetics*, IEEE ANTENNAS AND PROPAGATION MAGAZINE, IEEE ANTENNAS AND WIRELESS PROPAGATION LETTERS, and *Asian Information-Science-Life*.